EFFECTS OF MAGNETIC FIELD INCLINATION AND INTERNAL HEAT SOURCES ON NANOFLUID HEAT TRANSFER AND ENTROPY GENERATION IN A DOUBLE LID DRIVEN L-SHAPED CAVITY

by

Ali CHAMKHA[a], Zeinab ABDELRAHMAN[b], Mohamed MANSOUR[c], Taher ARMAGHANI[d*], and Ahmed RASHAD[e]

[a] Mechanical Engineering Department,
Prince Mohammad Endowment for Nanoscience and Technology,
Prince Mohammad Bin Fahd University, Al-Khobar, Saudi Arabia
[b] Basic and Applied Sciences Department, College of Engineering and Technology,
Arab Academy for Science and Technology and Maritime Transport,
Aswan Branch, Alexandria, Egypt
[c] Department of Mathematics, Faculty of Science, Assuit University, Assuit, Egypt
[d] Department of Engineering, Mahdishahr Branch, Islamic Azad University, Mahdishahr, Iran
[e] Department of Mathematics, Faculty of Science, Aswan University, Aswan, Egypt

Original scientific paper
https://doi.org/10.2298/TSCI190217325C

Mixed convection has been one of the most interesting subjects of study in the area of heat transfer for many years. The entropy generation due to MHD mixed convection heat transfer in L-shaped enclosure being filled with Cu-water nanofluid and having an internal heating generation is explored in this investigation by the finite volume technique. Lid-motion is presented by both right and top parts of walls to induce forced convection and the cavity is under an inclined uniform magnetic field along the positive horizontal direction. The statistics concentrated specifically on the impacts of several key parameters like as the aspect ratio of the enclosure, Hartmann number, nanoparticle volume fraction, and heat source length/location on the heat transfer inside the L-shaped enclosure. Outcomes have been manifested in terms of isotherm lines, streamlines, local and average Nusselt numbers. The obtained results show that addition of nanoparticles into pure fluid leads to increase of heat transfer. The maximum value of local Nusselt pertaining to the heat source occurs when L = 0.1. Impacts of heat source size and location, internal heat generation absorption, angle of magnetic field on heat transfer and entropy generation are completely analyzed and discussed. The best configuration and values of important parameters are also presented using thermal performance criteria.

Key words: *lid driven L-shaped enclosure, heat generation/absorption, nanofluid, entropy generation, heat source size/location, magnetic field*

Introduction

Mixed convection flow and heat transfer in cavities represent a significant phenomenon in science and engineering systems due to its wide applications in the operation of solar collectors, heat exchangers, drying technologies, home ventilation, high performance building insulation, and lubrication technologies. Mixed convection is more complicated compared to

* Corresponding author, e-mail: armaghani.taher@yahoo.com

other types of convection due to the coupling between the buoyancy force through temperature difference and the shear force due to the movement of wall. Using the change in the flow regime as well as adding nanoparticles with high thermophysical properties in the base fluid, called nanofluid, *i. e.* nanoparticles suspended in a pure fluid, which is one of the main candidates for cooling electronic devises, and of the possible ways for enhancing the mixed convection heat transfer. Therefore, some researchers have studied the nanofluid heat transfer in diverse shapes of cavities [1]. One of the very important types is the *L*-shaped enclosure. The following works address the nanofluid heat transfer in an *L*-shaped cavity. Mahmoodi [2] examined numerically the natural convective heat transfer of Cu-water nanofluid in an *L*-shaped enclosure. The results indicated that the mean Nusselt number increases with increment of the Rayleigh number and the nanofluid volume fraction in all ranges of the aspect ratio (AR). The MHD natural heat transfer of a nanofluid in an *L*-shaped cavity considering the magnetic field was considered by Sourtiji and Hosseinizadeh [3]. They communicated that the heat transfer reduced via enhancing the Hartmann number. Arani *et al.* [4] focused on the effects of inclination on Cu-water nanofluid natural convective heat transfer in an *L*-shaped cavity. They reported that the mean Nusselt number increased upon decreasing the shape factor and increasing the nanofluid volume fraction. The lattice-Boltzmann method (LBM) has been used by Mliki *et al.* [5] for simulation of nanofluid free convection heat transfer in an *L*-shaped cavity. Their obtained results showed an increment in the mean Nusselt number as a result of increasing the Rayleigh number. The effects of different nanoparticles on natural-convection of an *L*-shaped and an inverse *L*-shaped cavity have been investigated by Sidik *et al*. [6, 7]. Alavi *et al*. [8] and Armaghani *et al.* [9] studied the effects of a baffle on nanofluid heat transfer and entropy generation in an *L*-shaped cavity. They reported that by increasing the baffle length, the nanofluid had less impact on cooling in the cavity and as a result, the heat transfer raised. Recently, the authors extended their works by studying the nanofluid heat transfer and entropy generation in an *L*-shaped cavity with input and output ports [10, 11]. Their results showed that increasing the inclination angle led to a rise in heat transfer. It was clear that with the increase in the nanoparticles volume fraction, the thermal performance reduced, and that it increased when the inclination angle increased. The Al_2O_3-water nanofluid free convection in an *L*-shaped enclosure heated by a solid block was studied by Mohebbi and Rashidi [12] using LBM. They indicated that the maximum Nusselt number was observed as the heating block was situated at the bottom position inside the left wall. Recently, Rahimi *et al.* [13] considered the free convective heat transfer and entropy generation in a hollow *L*-shaped enclosure using LBM. They obtained some experimental values for thermophysical properties of a hybrid nanofluid and used it in their work.

Many authors also applied various configurations of cavities to improve the performance of thermofluid-flow systems by generating geometries and flow structures, and to study the process of self-optimization and self-organization in nature. The constructal statute reports that if a system has freedom to morph, it promotes in time the flow architecture that encourages simpler access to the currents that flow through it. Therefore, cavity protrusions are the vital developers of nucleate boiling and intensification considering the vapotron impact. In electronic cooling, cavities are utilized as the excess space occupied by the regular fins is a great concern. However, different configurations of the cavities were presented and geometrically optimized by Izadi *et al.* [1]. Rashad *et al.* [14], for example, presented and optimized *U*-shaped cavity. They elucidated that there existed an optimum geometrical framework of *U*-shaped cavity that decreased the temperature gradient to a minimum stage with the rise of the AR. They studied the effects of a partial slip condition on MHD nanofluid heat transfer in a *U*-shaped cavity for the first time.

Based on the literature and focusing on related reviews such as [1, 15], the combination of four topics (double lid driven *L*-shaped cavity, inclined magnetic field, internal heat generation/absorption, two discrete heat sources) is the main novelty of this paper. In this work, we depend on the constructed method in its main engineering importance, by concentrating on the optimization of geometry. The development of the rate of heat transfer is found to be more efficacious than the *U*-shaped cavity under the same volume fraction condition in the cavity. In this work, a Cu-water nanofluid is chosen because its cost is extremely low and copper is prevalent material and it can be intended easily. Analysis of mixed convection heat transfer and entropy generation of the current study is presented for the first time.

Mathematical formulation

The current configuration contains a 2-D *L*-shaped cavity as exhibited in fig. 1 with height AB and width BC remaining fixed at the same length, *H*. The thickness of the enclosure AF and CD are shown by *l* and the AR of the enclosure is noted by $L = l/H$. The top wall DE and the right wall EF of the cavity are lid-driven and moving at a constant velocity, U_0, in the positive/negative *x*- and *y*-directions, respectively. Both the top wall AF and the right wall CD of the enclosure are maintained at the cooled temperature, T_c, while the horizontal wall ED and the right wall EF are assumed to be adiabatic. Two heat sources with heat flux, q'', are placed on a portion of the left and the bottom walls of the enclosure with length, *b*, respectively while

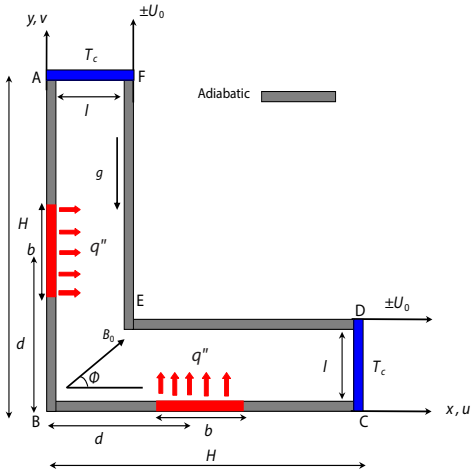

Figure 1. Scheme of the problem under the consideration

Table 1. Thermophysical properties of water and nanoparticle materials [14]

	ρ [kgm^{-3}]	c_p [Jkg^{-1}K^{-1}]	k [Wm^{-1}K^{-1}]	β [K^{-1}]	σ [μScm^{-1}]
Pure water	997.1	4179	0.613	$21 \cdot 10^{-5}$	0.05
Cu	8933	385	401	$1.67 \cdot 10^{-5}$	$5.96 \cdot 10^{7}$

the other remaining portions of these two walls are thermally insulated. The gravity is acting in the negative direction of the *y*-axis, and a magnetic field with strength, B_0, is applied on the left side of the cavity with angle, Φ, along the positive horizontal direction. The working fluid is Cu-water nanofluid with thermophysical properties are gathered in tab. 1, and it is considered to be steady Newtonian, laminar, and incompressible and is exposed to internal heat generation at a uniform rate, Q_0. The density variation in the nanofluid is approximated by the regular Boussinesq approximation. Therefore, the governing equations can be given in dimensional form, see [16, 17]:

$$\frac{\partial u}{\partial x}+\frac{\partial v}{\partial y}=0 \tag{1}$$

$$u\frac{\partial u}{\partial x}+v\frac{\partial u}{\partial y}=-\frac{1}{\rho_{\mathrm{nf}}}\frac{\partial p}{\partial x}+\nu_{\mathrm{nf}}\left(\frac{\partial^2 u}{\partial x^2}+\frac{\partial^2 u}{\partial y^2}\right)+\frac{\sigma_n B_0^2}{\rho_{\mathrm{nf}}}(v\sin\Phi\cos\Phi-u\sin^2\Phi) \tag{2}$$

$$u\frac{\partial v}{\partial x}+v\frac{\partial v}{\partial y}=-\frac{1}{\rho_{\mathrm{nf}}}\frac{\partial p}{\partial y}+\nu_{\mathrm{nf}}\left(\frac{\partial^2 v}{\partial x^2}+\frac{\partial^2 v}{\partial y^2}\right)+$$
$$+\frac{\sigma_{nf}B_0^2}{\rho_{nf}}(u\sin\Phi\cos\Phi-v\cos^2\Phi)+\frac{(\rho\beta)_{\mathrm{nf}}}{\rho_{\mathrm{nf}}}\mathrm{g}(T-T_{\mathrm{c}}) \tag{3}$$

$$u\frac{\partial T}{\partial x}+v\frac{\partial T}{\partial y}=\alpha_{\mathrm{nf}}\left(\frac{\partial^2 T}{\partial x^2}+\frac{\partial^2 T}{\partial y^2}\right)+\frac{Q_0}{(\rho c_p)_{\mathrm{nf}}}(T-T_{\mathrm{c}}) \tag{4}$$

The boundary conditions imposed on the problem are taken as:

$$\begin{gathered}
x=0,\ u=v=0,\frac{\partial T}{\partial x}=-\frac{q''}{k_{\mathrm{nf}}},\ (d-0.5b)\le y\le(d+0.5b),\ \text{and}\ \frac{\partial T}{\partial x}=0,\ \text{otherwise}\\
y=0,\ u=v=0,\frac{\partial T}{\partial y}=-\frac{q''}{k_{\mathrm{nf}}},\ (d-0.5b)\le x\le(d+0.5b),\ \text{and}\ \frac{\partial T}{\partial y}=0,\ \text{otherwise}\\
x=l,\ u=0,\ \ v=\lambda_l U_0,\ \ \frac{\partial T}{\partial x}=0,\ x=H,\ \ u=v=0,\ \ T=T_{\mathrm{c}}\\
y=l,\ \ v=0,\ \ u=\lambda_d U_0,\ \ \frac{\partial T}{\partial y}=0,\ \ y=H,\ \ u=v=0,\ \ T=T_{\mathrm{c}}
\end{gathered} \tag{5}$$

where ρ_{nf}, $(\rho c_p)_{\mathrm{nf}}$, $(\rho\beta)_{\mathrm{nf}}$, μ_{nf}, α_{nf} are defined, see [18-22]:

$$\rho_{\mathrm{nf}}=(1-\phi)\rho_{\mathrm{f}}+\phi\rho_{\mathrm{p}} \tag{6}$$

$$(\rho c_p)_{\mathrm{nf}}=(1-\phi)(\rho c_p)_{\mathrm{f}}+\phi(\rho c_p)_{\mathrm{p}} \tag{7}$$

$$(\rho\beta)_{\mathrm{nf}}=(1-\phi)(\rho\beta)_{\mathrm{f}}+\phi(\rho\beta)_{\mathrm{p}} \tag{8}$$

$$\alpha_{\mathrm{nf}}=\frac{k_{\mathrm{nf}}}{(\rho c_{\mathrm{p}})_{\mathrm{nf}}},\quad \frac{k_{\mathrm{nf}}}{k_{\mathrm{f}}}=\frac{(k_{\mathrm{p}}+2k_{\mathrm{f}})-2\phi(k_{\mathrm{f}}-k_{\mathrm{p}})}{(k_{\mathrm{p}}+2k_{\mathrm{f}})+\phi(k_{\mathrm{f}}-k_{\mathrm{p}})} \tag{9}$$

$$\mu_{\mathrm{nf}}=\frac{\mu_f}{(1-\phi)^{2.5}},\quad \frac{\sigma_{\mathrm{nf}}}{\sigma_{\mathrm{f}}}=1+\frac{3(\gamma-1)\phi}{(\gamma+2)-(\gamma-1)\phi},\quad \gamma=\frac{\sigma_{\mathrm{p}}}{\sigma_{\mathrm{f}}} \tag{10}$$

Introducing the following dimensionless set:

$$\begin{gathered}
X=\frac{x}{H},\ \ Y=\frac{y}{H},\ \ U=\frac{u}{U_0},\ \ V=\frac{v}{U_0},\ \ P=\frac{p}{\rho_{\mathrm{nf}}U_0^2}\\
\theta=\frac{(T-T_c)}{\Delta T},\ \ \mathrm{Ri}=\frac{\mathrm{Gr}}{\mathrm{Re}^2},\ \ \Delta T=\frac{q''H}{k_{\mathrm{f}}}
\end{gathered} \tag{11}$$

into eqs. (1)-(4), yields the following dimensionless equations:

$$\frac{\partial U}{\partial X}+\frac{\partial V}{\partial Y}=0 \tag{12}$$

$$U\frac{\partial U}{\partial X}+V\frac{\partial U}{\partial Y}=-\frac{\partial P}{\partial X}+\frac{1}{\mathrm{Re}}\left(\frac{\nu_{\mathrm{nf}}}{\nu_{\mathrm{f}}}\right)\left(\frac{\partial^2 U}{\partial X^2}+\frac{\partial^2 U}{\partial Y^2}\right)+\left(\frac{\rho_{\mathrm{f}}}{\rho_{\mathrm{nf}}}\right)\left(\frac{\sigma_{\mathrm{nf}}}{\sigma_{\mathrm{f}}}\right)\frac{\mathrm{Ha}^2}{\mathrm{Re}}(V\sin\Phi\cos\Phi-U\sin^2\Phi) \tag{13}$$

$$U\frac{\partial V}{\partial X}+V\frac{\partial V}{\partial Y}=-\frac{\partial P}{\partial Y}+\frac{1}{\mathrm{Re}}\left(\frac{\nu_{\mathrm{nf}}}{\nu_{\mathrm{f}}}\right)\left(\frac{\partial^2 V}{\partial X^2}+\frac{\partial^2 V}{\partial Y^2}\right)+\mathrm{Ri}\frac{(\rho\beta)_{\mathrm{nf}}}{\rho_{\mathrm{nf}}\beta_{\mathrm{f}}}\theta+$$
$$+\left(\frac{\rho_{\mathrm{f}}}{\rho_{\mathrm{nf}}}\right)\left(\frac{\sigma_{\mathrm{nf}}}{\sigma_{\mathrm{f}}}\right)\frac{\mathrm{Ha}^2}{\mathrm{Re}}(U\sin\Phi\cos\Phi-V\cos^2\Phi) \tag{14}$$

$$U\frac{\partial\theta}{\partial X}+V\frac{\partial\theta}{\partial Y}=\left(\frac{1}{\mathrm{Pr}\,\mathrm{Re}}\right)\frac{\alpha_{\mathrm{nf}}}{\alpha_{\mathrm{f}}}\left(\frac{\partial^2\theta}{\partial X^2}+\frac{\partial^2\theta}{\partial Y^2}\right)+\frac{1}{\mathrm{Re}\,\mathrm{Pr}}\frac{(\rho c_p)_{\mathrm{f}}}{(\rho c_p)_{\mathrm{nf}}}Q\theta \tag{15}$$

$$\mathrm{Pr}=\frac{\nu_{\mathrm{f}}}{\alpha_{\mathrm{f}}},\ \ \mathrm{Re}=\frac{U_0 H}{\nu_{\mathrm{f}}},\ \ \mathrm{Gr}=\frac{\mathrm{g}\beta_{\mathrm{f}} H^3\Delta T}{\nu_f^2},\ \ \mathrm{Ha}=B_0 H\sqrt{\frac{\sigma_{\mathrm{f}}}{\mu_{\mathrm{f}}}} \tag{16}$$

where Pr is the Prandtl number, Re – the Reynolds number, Gr – the Grashof number, and Ha – Hartmann number, respectively.

The dimensionless boundary condition for eqs. (12)-(15):

$$X=0,\ U=V=0,\ \frac{\partial\theta}{\partial X}=-\frac{k_{\mathrm{f}}}{k_{\mathrm{nf}}},\ (D-0.5B)\le Y\le(D+0.5B),\ \text{and}\ \frac{\partial\theta}{\partial X}=0,\ \text{otherwise}$$
$$Y=0,U,\ V=0,\ \frac{\partial\theta}{\partial Y}=-\frac{k_f}{k_{nf}},\ (D-0.5B)\le X\le(D+0.5B),\ \text{and}\ \frac{\partial\theta}{\partial Y}=0,\ \text{otherwise} \tag{17}$$
$$X=L,\ U=0,\ V=\lambda_l,\ \frac{\partial\theta}{\partial X}=0,\ X=1,\ U=V=0,\ \ \theta=0$$
$$Y=L,\ V=0,\ U=\lambda_d,\ \frac{\partial\theta}{\partial Y}=0,\ Y=1,\ U=V=0,\ \theta=0$$

The local Nusselt number is defined:

$$(\mathrm{Nu}_s)_{Y=0}=\frac{1}{\theta_s(X)},\quad (\mathrm{Nu}_s)_{X=0}=\frac{1}{\theta_s(Y)} \tag{18}$$

and the average Nusselt number is defined:

$$\mathrm{Nu}_m=\frac{1}{B}\left[\int_{D-0.5B}^{D+0.5B}(\mathrm{Nu}_s)_{Y=0}\,\mathrm{d}X+\int_{D-0.5B}^{D+0.5B}(\mathrm{Nu}_s)_{X=0}\,\mathrm{d}Y\right] \tag{19}$$

Entropy generation analysis

Following [23-25] and the local thermodynamic equilibrium of the linear transport theory, the dimensionless total local entropy generation can be expressed:

$$S=s\frac{H^2}{k_{\mathrm{f}}}=\frac{1}{(\theta+C_T)^2}\left(\frac{k_{\mathrm{nf}}}{k_{\mathrm{f}}}\right)\left[\left(\frac{\partial\theta}{\partial X}\right)^2+\left(\frac{\partial\theta}{\partial Y}\right)^2\right]+\frac{\Theta}{(\theta+C_T)}\mathrm{Re}^2\mathrm{Pr}^2\left(\frac{\mu_{\mathrm{nf}}}{\mu_{\mathrm{f}}}\right).$$
$$\cdot\left\{2\left[\left(\frac{\partial U}{\partial X}\right)^2+\left(\frac{\partial V}{\partial Y}\right)^2\right]+\left(\frac{\partial V}{\partial X}+\frac{\partial U}{\partial Y}\right)^2\right\}+\frac{\Theta}{(\theta+C_T)}\mathrm{Re}^2\,\mathrm{Pr}^2\,.$$
$$\cdot\left(\frac{\sigma_{\mathrm{nf}}}{\sigma_{\mathrm{f}}}\right)\mathrm{Ha}^2(U\sin\Phi-V\cos\Phi)^2=Sh+Sv+Sj \tag{20}$$

where

$$\Theta = \left(\frac{\mu_f}{\Delta T k_f}\right)\left(\frac{\alpha_f}{H}\right)^2$$

Here, *Sh*, *Sv*, and *S*j are the dimensionless local entropy generation rate due to heat transfer, fluid fraction and Joule heating, respectively.

Also, the following Nusselt number ratio, total entropy generation ratio and the thermal performance criteria reported by Ismael *et al.* [26] are defined:

$$\mathrm{Nu}_m^+ = \frac{\mathrm{Nu}_m}{(\mathrm{Nu}_m)_{\phi=0}} \quad \text{and} \quad \mathrm{Nu}_m^{++} = \frac{\mathrm{Nu}_m}{(\mathrm{Nu}_m)_{\mathrm{Ha}=0}} \tag{21}$$

$$S^+ = \frac{S}{(S)_{\phi=0}} \quad \text{and} \quad S^{++} = \frac{S}{(S)_{\mathrm{Ha}=0}} \tag{22}$$

$$e^+ = \frac{S^+}{\mathrm{Nu}_m^+} \quad \text{and} \quad e^{++} = \frac{S^{++}}{\mathrm{Nu}_m^{++}} \tag{23}$$

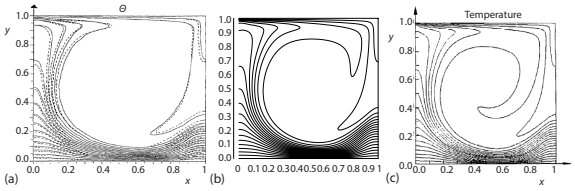

Figure 2. Comparison of the present study with Re = 1000, Pr = 0.71, Gr = 10^2, ϕ = 0; (a) [16], (b) present study, and (c) [17]

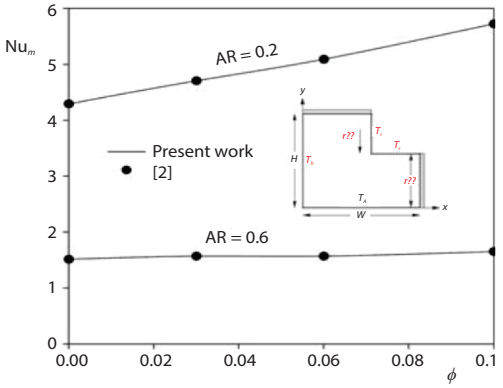

Figure 3. Code validation with the *L*-shaped enclosure of Mahmoodi [2]

Numerical solution and validation

The conservation eqs. (12)-(15) in conjunction with the associated boundary conditions (17) elucidate a system of non-linear PDE that are strongly coupled. These equations are transformed into algebraic equations through the finite volume approach and then are solved iteratively by the tridiagonal matrix algorithm, utilizing the SIMPLE algorithm [27]. Figure 2 shows the results of the current code compared with those of Khanafar *et al.* [16] and Iwatsu *et al.* [17]. The outputs demonstrate an assent between this study and the previously published studies.

Also, for more validation of the *L*-shaped cavity, a comparison between the present work and that of Mahmoodi [2] is presented in fig. 3 and the result shows very good agreement.

For convergence, the under-relaxation technique has been employed. The iteration is performed until the normalized residuals of the mass, momentum, temperature, and entropy generation equations become less than 10^{-6}. Non-uniform grids containing of 101 × 101 grid nodes in the *X*- and *Y*-directions, respectively, are used. The obtained data are independent of the number of grids. The grid independency data are found at Ha = 10, Θ = 10^{-3}, C_T = 0.1, Gr = 10^4, Re = 10, *D* = 0.5, *B* = 0.5, *Q* = 1.0, *Φ* = 45, ϕ = 0.05, $\lambda_1 = -\lambda_d = 1.0$, and displayed in tab. 2.

Table 2. Grid-independency study for Cu-water nanofluid

Grid-size	41 × 41	61 × 61	81 × 81	91 × 91	101 × 101	121 × 121
Nu_m	1.469836	1.448858	1.437232	1.429925	1.424576	1.424554

Results and discussion

In the present work, a representative set of numerical results is obtained at the fixed parameters $\Theta = 10^{-3}$, $C_T = 0.1$, Gr = 10^4, Re = 10, and $\lambda_1 = -\lambda_d = 1.0$

Effect of aspect ratio

Figure 4 presents isothermal lines as well as streamlines for various AR. The heat sources at the bottom and the left walls account for the upward movement and the counter clockwise (CW) rotation of the nanofluid since it becomes lighter due to the change of density. The moving plates and the nanofluid move in opposite directions. However, their impact decreases for large values of L and hence, the nanofluid rotates faster. For $L = 0.1$, in the region above the cavity, the isothermal lines are horizontal and nearly parallel, while under the cavity, they are vertical and nearly parallel. The proximity of the plates of the cavity is regarded as a reason. The isothermal lines assume a parabolic shape and become nearly parallel as the distances between the plates L increases.

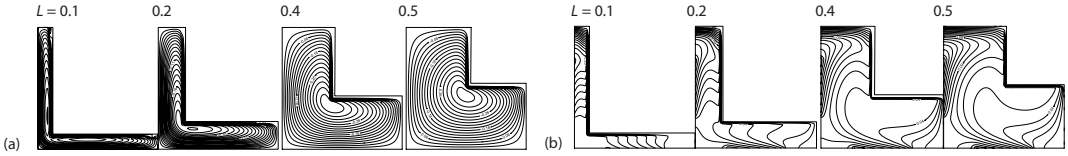

Figure 4. (a) Streamlines and (b) isothermal lines for different values of L, at Ha = 10, D = 0.5, B = 0.5, Q = 1.0, ϕ = 0.05, Φ = 45°

Figure 5 shows the local Nusselt number for different values of L. As mentioned earlier, two local Nusselt numbers have been presented in this work since there are two heat sources. Considering the isothermal lines indicated in fig. 4, as the fluid-flows over the lower heat source, the temperature of the nanofluid decreases due to its CW rotation. As a result, taking the definition of local Nusselt number into account, the Nusselt number increases. The maximum value of the local Nusselt number pertaining to the heat source occurs when $L = 0.1$. The reverse process is observed at the heat source of the left wall. The difference is that at the end of wall, the decrease of the local Nusselt is more noticeable for $L = 0.1$. Its cause, as explained in fig. 4, is the shape of isothermal lines.

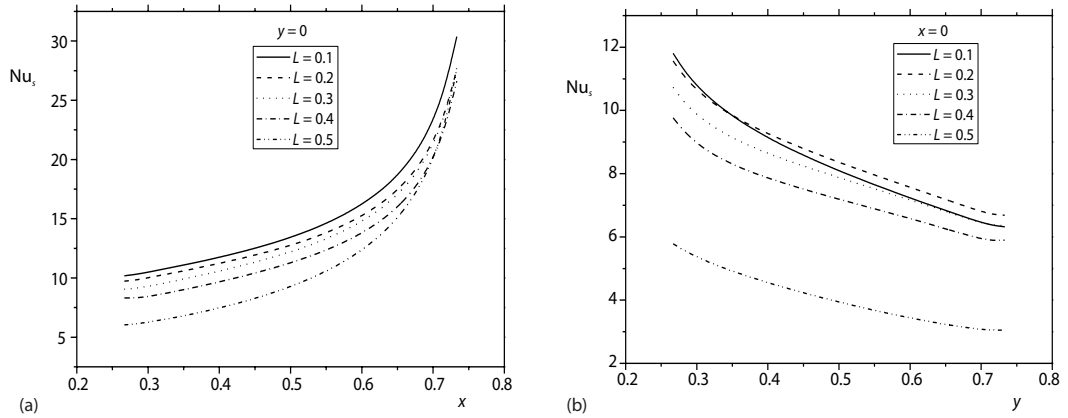

Figure 5. Local Nusselt number along the heat source various AR at Ha = 10, D = 0.5, B = 0.5, Q = 1.0, ϕ = 0.05, Φ = 45°

Figure 6 shows Nu_m and Nu_m^+ for different values of L, and based on the variations of the volume fraction ϕ. As evident in this figure, for all values of L, the Nusselt number increases with the rise of ϕ and becomes maximum at $L = 0.1$, while the maximum rate of heat transfer growth with the increase of ϕ occurs at $L = 0.2$. The increase of heat transfer also leads to increase of irreversibility thereof and hence, the entropy increases with the rise of ϕ, fig. 7(a).

Figure 7(b) presents Nu_m^{++} for different values of Hartmann number and L. For L = 0.1 to 0.3, the Nusselt number increases with the increase of Hartmann number from zero to about 20, while it does not change noticeably up to Ha = 50. For $L = 0.4$, with the increase of Hartmann number, the Nusselt number increases slightly, while for $L = 0.5$, the Nusselt number decreases slightly with the increase of Hartmann number.

Figure 8 shows e^{++} for different values of L and based on variation of Hartmann number. As seen in the figure, an increase of Hartmann number up to 20 causes an improvement in the thermal performance for all values of L, whereas it decreases when Hartmann number increases to 50. It can generally be claimed that at $L = 0.1$, the thermal performance improves for all values of Hartmann number. The most efficient value of Hartmann number is 15 since e^{++} has the minimum value at this Hartmann number value.

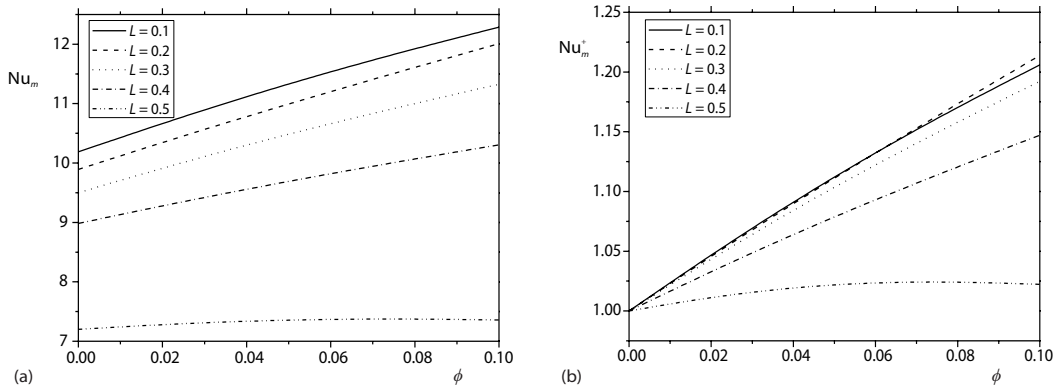

Figure 6. Variation of the average Nu_m and Nu_m^+ for different values of L, at Ha = 10, $D = 0.5$, $B = 0.5$, $Q = 1.0$, $\Phi = 45°$

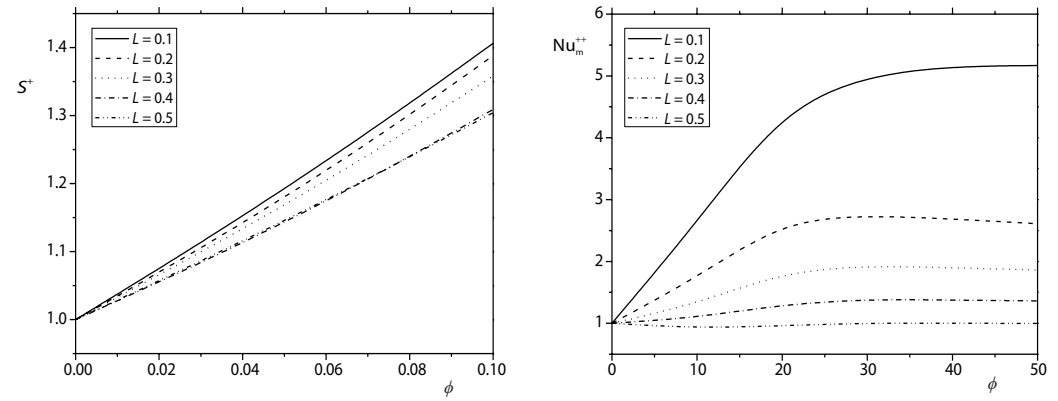

Figure 7. Variation of the average total entropy generation and average Nusselt number for different values of L at $D = 0.5$, $B = 0.5$, $Q = 1.0$, $\Phi = 45°$

Effect of heat source size

Figure 9 shows the effects of the size of heat source on the streamlines and the isothermal lines. With the increase of heat source size, the streamlines do not change noticeably, while the temperature of wall of the heat source increases and the Nusselt number decreases, figs. 10(a) and 10(b).

Figure 10(c) shows the variations of the average Nusselt number with ϕ and based on different values of B. The maximum value of the average Nusselt number is observed at $B = 0.1$, while the minimum value is seen at $B = 0.8$. In general, addition of nanoparticles into pure fluids causes an increase in the average Nusselt

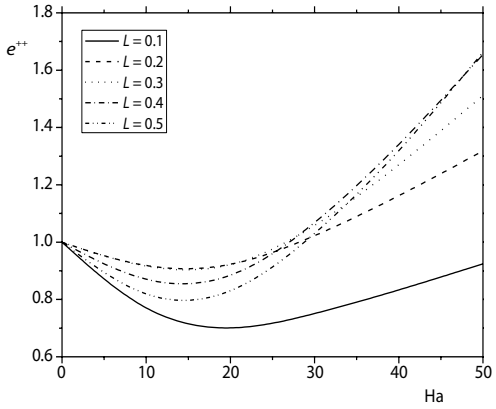

Figure 8. Variation of global entropy to average Nusselt number for different values of L at $D = 0.5$, $B = 0.5$, $Q = 1.0$, $\phi = 0.05$, $\Phi = 45°$

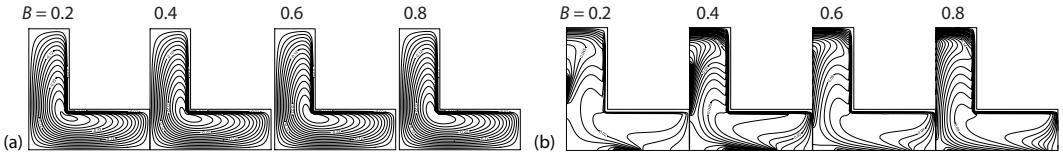

Figure 9. (a) Streamlines and (b) isothermal lines for different values of B at Ha = 10, $D = 0.5$, $L = 0.3$, $Q = 1.0$, $\phi = 0.05$, $\Phi = 45°$

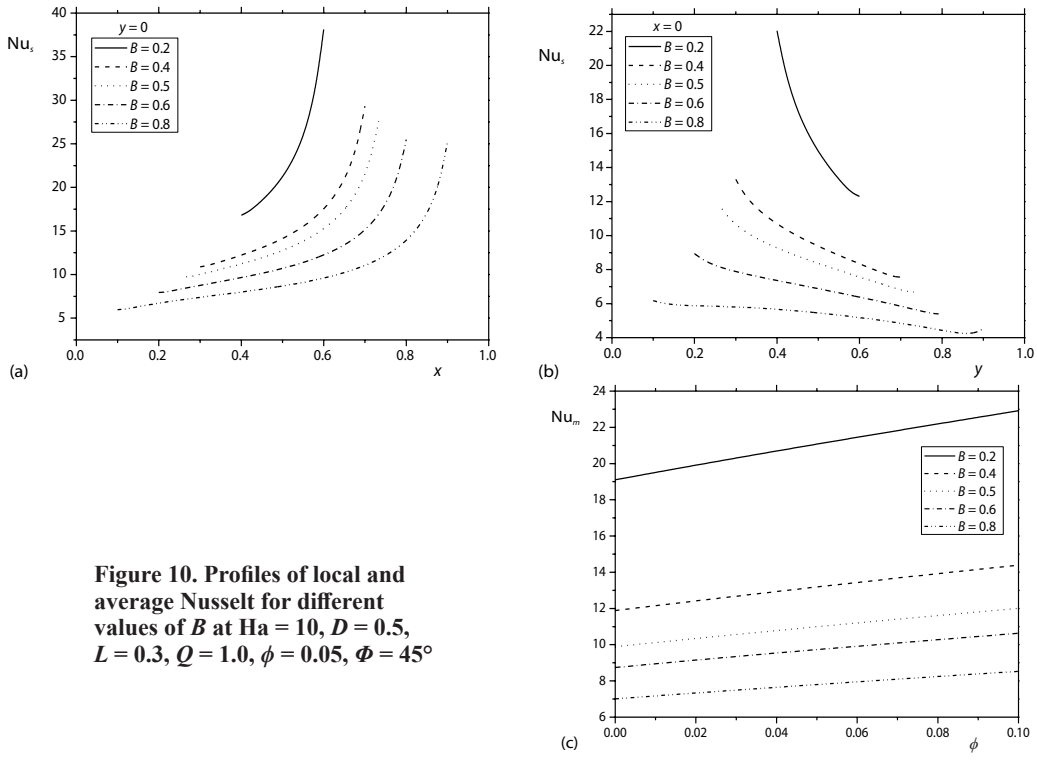

Figure 10. Profiles of local and average Nusselt for different values of B at Ha = 10, $D = 0.5$, $L = 0.3$, $Q = 1.0$, $\phi = 0.05$, $\Phi = 45°$

number for all values of B. As mentioned earlier, an increase of the Nusselt number also leads to an increase in the irreversibility due to heat transfer, and therefore, causes an increase in the entropy generation.

Figures 11(a) and 11(c) show the changes of the Nusselt number for various values of B, and based on the increases of Hartmann number. The trend of variation of the Nusselt number with Hartmann number may be divided into two ranges: Ha = 0-25 and Ha = 25-50. For small values of Hartmann number, the average Nusselt number increases with the increase of Hartmann number, while for values of Hartmann number above 25, an increase of Hartmann number, not only has a negligible effect on heat transfer, but also leads to its slight decrease for small values of B.

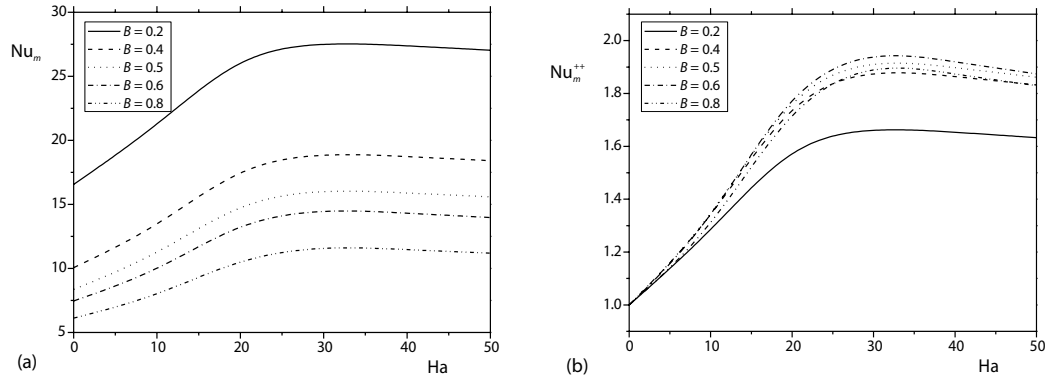

Figure 11. Variation of the average Nusselt number for different values of B at $D = 0.5$, $L = 0.3$, $Q = 1.0$, $\phi = 0.05$, $\Phi = 45°$

As indicated in fig. 12(a), an increase of Hartmann number leads to an increase of entropy. Figure 12(b) shows the variation of e^{++} with Hartmann number. Increasing the value of Hartmann number causes an improvement in the thermal performance for all values of B and for Hartmann number values less than 20. While for values above 20, it leads to a loss in the thermal performance.

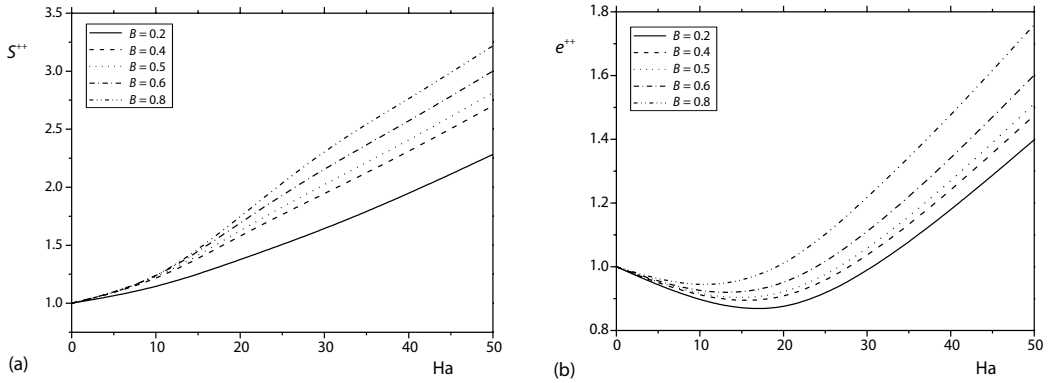

Figure 12. Average total entropy generation and thermal performance criteria for different values of B at $D = 0.5$, $L = 0.3$, $Q = 1.0$, $\phi = 0.05$, $\Phi = 45°$

Effects of angle of magnetic field and heat generation parameter

In fig. 13, the streamlines and isothermal lines are presented for various angles of the magnetic field. The effects of different angles of the magnetic field are more on the isothermal lines than on the streamlines, so that an increase of this angle causes an increase in the temperature of the fluid adjacent to the heat source and therefore, the heat transfer and Nusselt number increase, fig. 14.

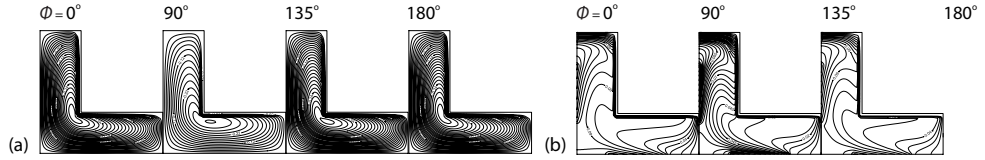

Figure 13. (a) Streamlines and (b) isothermal lines (b) for different values of Φ at Ha = 10, D=0.5, B = 0.5, L = 0.3, Q = 1.0, ϕ = 0.05

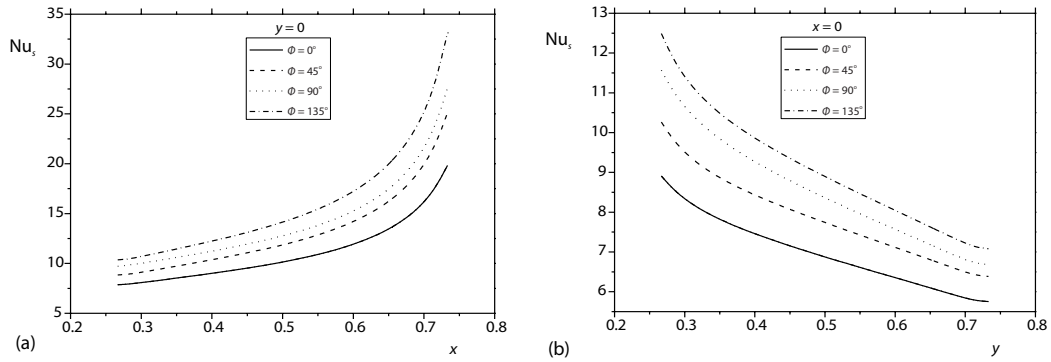

Figure 14. Local Nusselt number along the heat source for different values of Φ at Ha = 10, D = 0.5, B = 0.5, L = 0.3, Q = 1.0, ϕ = 0.05

Figures 15(a) and 15(b) show the average Nusselt number for various amounts of ϕ and Φ. For all angles of the applied magnetic field, an increase of the volume fraction leads to an increase in the Nusselt number. The increase is maximized at the angle of 135°, so that with the addition of nanoparticles for 10 vol.%, the heat transfer increases more than 20%. Figure 15(c) shows the Nusselt number for different values of Q. The maximum and minimum values of the Nusselt number are observed at Q = –2 and Q = 2, respectively.

A similar trend is seen in fig. 16(a) for Nu_m^+. In general, an addition of nanoparticles causes an increase of the heat transfer for all values of Q, while the rate of increment is maximum for Q = 2. More than 25% increment of heat transfer is observed for Q = 2 and ϕ = 0.1. Considering the role of irreversibility due to heat transfer on the entropy generation, for all values of Q, the total entropy generation increases with the increase of the volume fraction which is maximum when Q = 2, fig. 16(b).

Conclusions

The entropy generation due to MHD mixed convection heat transfer in an L-shaped enclosure being filled with a Cu-water nanofluid and having an internal heat generation is studied numerically in this paper by the finite volume technique. The remarkable results are:

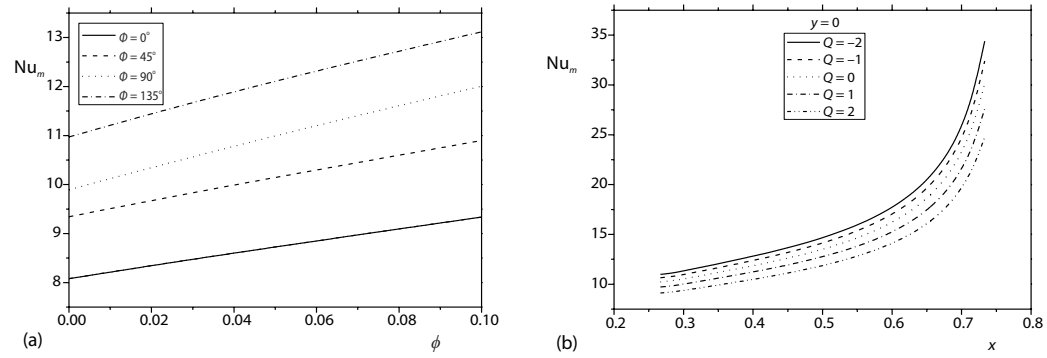

Figure 15. Average Nusselt number and local Nusselt number for different values of Q at Ha = 10, D = 0.5, B = 0.5, L = 0.3, ϕ = 0.05, Φ = 45°

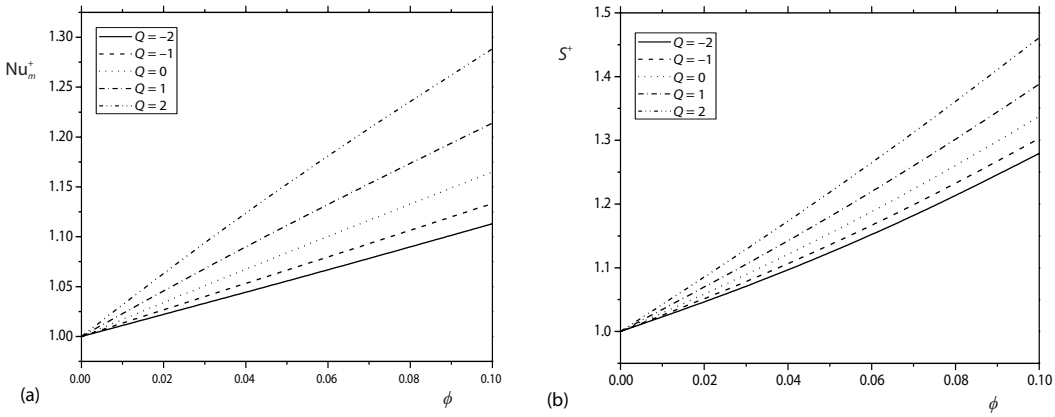

Figure 16. Variation of the average Nusselt number and variation of the average total entropy generation for different values of Q at Ha = 10, D = 0.5, B = 0.5, L = 0.3, Φ = 45°

- For all amounts of L, the Nusselt number increases with the rise of ϕ and becomes maximum at L = 0.1.
- For L = 0.1 to 0.3, the Nusselt number increases with the increase of Hartmann number from zero to about 20, while it will not change noticeably up to Ha = 50.
- The maximum value of the average Nusselt number is observed at B = 0.1, while the minimum value is seen at B = 0.8.
- For a volume fraction of 0.1, an increase of about 20% in heat transfer is observed for D = 0.3.

- The maximum and minimum values of the Nusselt number are observed at $Q = -2$ and $Q = 2$, respectively.
- For all angles of the applied magnetic field, an increase of the volume fraction leads to an increase of the Nusselt number.
- The entropy generation increases with the rise of ϕ.

Nomenclature

B – dimensionless heat source length, [–]
b – length of heat source, [m]
B_0 – magnetic field strength, [T]
c_p – specific heat, [JkgK^{-1}]
C_T – difference temperature, [–]
D – dimensionless heat source position, [–]
d – location of heat source, [m]
Gr – Grashof number, [–]
g – acceleration due to gravity, [ms^{-2}]
H – length of cavity, [m]
Ha – Hartmann number, [–]
k – thermal conductivity, [Wm^{-1}K^{-1}]
L – aspect ratio, [–]
l – thickness of the enclosure, [m]
Nu$_s$ – local Nusselt number of heat source, [–]
Nu$_m$ – average Nusselt number, [–]
P – dimensionless pressure, [–]
Pr – Prandtl number, [–]
p – fluid pressure, [Pa]
Q – dimensionless heat generation coefficient, [–]
Q_o – Heat generation coefficient, [Wm^{-2}]
q" – heat flux, [Wm^{-2}]
Re – Reynolds number, [–]
S – entropy generation, [WK^{-1}m^{-1}]
T – temperature, [K]
T_c – cold wall temperature, [K]
u, v – velocity components in x, y directions, [ms^{-1}]
U, V – dimensionless velocity components, [–]
x, y – Cartesian co-ordinates, [m]
X, Y – dimensionless co-ordinates, [–]

Greek symbols

α – thermal diffusivity, [m^{2}s^{-1}]
β – thermal expansion coefficient, [K^{-1}]
θ – dimensionless temperature, [–]
μ – dynamic viscosity, [kgm^{-1}s^{-1}]
ν – kinematic viscosity, [m^{2}s^{-1}]
ρ – density, [kgm^{-3}]
σ – effective electrical conductivity, [Sm^{-1}]
Φ – angle of magnetic field, [°]
ϕ – solid volume fraction, [–]

Subscripts

c – cold
f – pure fluid
h – hot
m – average
nf – nanofluid
p – nanoparticle

References

[1] Izadi, S., *et al*., A Comprehensive Review on Mixed Convection of Nanofluids in Various Shapes of Enclosures, *Powder Technology*, *343* (2019), 2, pp. 880-907
[2] Mahmoodi, M., Numerical Simulation of Free Convection of a Nanofluid in L-Shaped Cavities, *International Journal of Thermal Sciences*, *50* (2011), 9, pp. 1731-1740
[3] Sourtiji, E., Hosseinizadeh, S. F., Heat Transfer Augmentation of Magnetohydrodynamics Natural-Convection in L-Shaped Cavities Utilizing Nanofluid, *Thermal Science*, *16* (2012), 2, pp. 489-501
[4] Abbasian Arani, A. A., *et al*., Study of Nanofluid Natural-Convection in an Inclined L-Shaped Cavity, *Scientia Iranica*, *20* (2013), 6, pp. 2297-2305
[5] Mliki, B., *et al*, Lattice-Boltzmann Simulation of Natural-Convection in an L-Shaped Enclosure in the Presence of Nanofluid, *Inter. J. Engineering Science and Technology*, *18* (2015), 3, pp. 503-511
[6] Che Sidik, N. A., *et al*., Numerical Investigation of Natural-Convection of Nanofluids in L-Shaped Enclosures, *Advanced Materials Research*, *849* (2013), Nov., pp. 391-396
[7] Che Sidik, N. A., *et al*., Modelling of Convective Heat Transfer of Nanofluid in Inversed L-Shaped Cavities, *Journal of Advanced Research in Fluid Mechanics and Thermal Sciences*, *21* (2016), 1, pp. 1-12
[8] Alavi, N., *et al*., Natural-Convection Heat Transfer of a Nanofluid in a Baffle L-Salped Cavity, *Journal of Solid and Fluid Mechanics*, *6* (2016), 4, pp. 311-321
[9] Armaghani, T., *et al*., Numerical Investigation of Water-Alumina Nanofluid Natural-Convection Heat Transfer and Entropy Generation in a Baffled L-Shaped Cavity, *Journal of Molecular Liquids*, *223* (2016), 11, pp. 243-251

[10] Armaghani, T., *et a*l., Mixed Convection and Entropy Generation of an Ag-Water Nanofluid in an Inclined L-Shaped Channel, *Energies*, *12* (2019), 6, pp. 1150-1160
[11] Armaghani, T., *et al*., Effects of Discrete Heat Source Location on Heat Transfer and Entropy Generation Nanofluid in an Open Inclined L-Shaped Cavity, *International Journal of Numerical Methods for Heat and Fluid-Flow*, *29* (2019), 4, pp. 1363-1377
[12] Mohebbi, R., *et al.*, Numerical Simulation of Natural-Convection Heat Transfer of a Nanofluid in an L -Shaped Enclosure with a Heating Obstacle, *Journal of the Taiwan Institute of Chemical Engineers*, *72* (2017), 3, pp. 70-84
[13] Rahimi, A., *et al.*, Natural-Convection Analysis Employing Entropy Generation and Heatline Visualization in a Hollow L-Shaped Cavity Filled with Nanofluid Using Lattice Boltzmann Method- Experimental Thermo-Physical Properties, *Physica E: Low-Dimensional Systems and Nanostructures*, *97* (2018), 3, pp. 82-97
[14] Rashad, A. M., *et al*., The MHD Mixed Convection and Entropy Generation of Nanofluid in a Lid-Driven U-Shaped Cavity with Internal Heat and Partial Slip, *Physics of Fluids*, *31* (2019), 4, 042006
[15] Mohamad, A. T., *et al*., Nanoparticles: A Review on Their Synthesis, Characterization and Physicochemical Properties for Energy Technology Industry, *Journal of Advanced Research in Fluid Mechanics and Thermal Sciences*, *46* (2018), 1, pp. 1-10
[16] Khanafer, K. M, *et al*., Mixed Convection Flow in a Lid-Driven Enclosure Filled with a Fluid-Saturated Porous Medium, *International Journal of Heat and Mass Transfer*, *42* (1999), 13, pp. 2465-2481
[17] Iwatsu, R., *et al.*, Mixed Convection in a Driven Cavity with a Stable Vertical Temperature Gradient, *International Journal of Heat and Mass Transfer*, *36* (1993), 6, pp. 1601-1608
[18] Aminossadati, S. M., *et al*., Natural-Convection Cooling of a Localized Heat Source at the Bottom of a Nanofluid-Filled Enclosure, *Eur. J. Mech. B/Fluids*, *28* (2009), 5, pp. 630-40
[19] Khanafer, K. M., *et al*., Buoyancy-Driven Heat Transfer Enhancement in a 2-D Enclosure Utilizing Nanofluids, *International Journal of Heat and Mass Transfer*, *46* (2003), 19, pp. 3639-3653
[20] Abu-Nada, E., *et al.*, Effect of Nanofluid Variable Properties on Natural-Convection in Enclosures Filled with a Cuo-EG-Water Nanofluid, *International Journal of Thermal Sciences*, *49* (2010),12, pp. 2339-2352
[21] Maxwell, J. A., *Treatise on Electricity and Magnetism*, 2nd ed., Oxford University, Press, Cambridge, UK, 1904
[22] Brinkman, H. C., The Viscosity of Concentrated Suspensions and Solution, *Jornal of Chemical Physics*, *20* (1952), 4, pp. 571-581
[23] Chamkha, A. J., *et al*., Effects of Heat Sink and Source and Entropy Generation on MHD Mixed Convection of a Cu-Water Nanofluid in a Lid-Driven Square Porous Enclosure with Partial Slip, *Physics of Fluids*, *29* (2017), 5, 052001
[24] Chamkha, A. J., *et al*., Effects of Partial Slip on Entropy Generation and MHD Combined Convection in a Lid-Driven Porous Enclosure Saturated with a Cu–Water Nanofluid, *Journal of Thermal Analysis and Calorimetry*, *132* (2018), 2, pp. 1291-1306
[25] Rashad, A. M., *et al*., Entropy Generation and MHD Natural-Convection of a Nanofluid in an Inclined Square Porous Cavity: Effects of a Heat Sink and Source Size and Location, *Chinese Journal of Physics*, *56* (2018), 1, pp. 193-211
[26] Ismael, M. A., *et al.*, Conjugate Heat Transfer and Entropy Generation in a Cavity Filled with a Nanofluid-Saturated Porous Media and Heated by a Triangular Solid, *Journal of the Taiwan Institute of Chemical Engineering*, *59* (2016), 2, pp. 138-151
[27] Patankar, S. V., *Numerical Heat Transfer and Fluid-Flow*, Hemisphere, New York, USA, 1980

Paper submitted: February 17, 2019
Paper revised: July 21, 2019
Paper accepted: August 15, 2019